# Textural and chemical changes in slate-forming phyllosilicates across the external-internal zones transition in the low-grade metamorphic belt of the NW Iberian Variscan Chain

Autor(en): **Abad, Isabel / Nieto, Fernando / Gutiérrez-Alonso, Gabriel**

Objekttyp: **Article**

Zeitschrift: **Schweizerische mineralogische und petrographische Mitteilungen = Bulletin suisse de minéralogie et pétrographie**

Band (Jahr): **83 (2003)**

Heft 1

PDF erstellt am: **11.09.2024**

Persistenter Link: https://doi.org/10.5169/seals-63136

*Schweizerische Mineralogische und Petrographische Mitteilungen 83, 63–80, 2003*

# Textural and chemical changes in slate-forming phyllosilicates across the external-internal zones transition in the low-grade metamorphic belt of the NW Iberian Variscan Chain

*Isabel Abad*[1], *Fernando Nieto*[2] and *Gabriel Gutiérrez-Alonso*[3]

**Abstract**

Differences in the chemistry and texture of slate-forming phyllosilicates representative of foreland and hinterland rocks of the Iberian Variscan Orogenic Belt have been determined by scanning and transmission electron microscopy. Based on a previous X-ray diffraction study, representative samples of both internal and external domains were selected revealing clearly different characteristics. The two samples corresponding to the foreland rocks have similar texture, showing a mixture of sedimentary and metamorphic features at the backscattered electron scale, independently of their respective epizone and anchizone illite crystallinity indices. At the crystalline lattice level, mica and chlorite packets form sub-parallel low-angle intergrowths and show strain features, more obvious in chlorite than in mica. The only difference justifying their different crystallinity indices concerns quantitative characteristics such as crystallite size and frequency of defects. The two hinterland samples are very similar and are formed by perfect, defect-free micrometer-size phyllosilicates in a typically metamorphic parallel orientation. The foreland samples are chemically heterogeneous, with each individual analysis being affected by variable degrees of illitic, phengitic and ferrimuscovitic substitutions. In contrast, the hinterland samples have evolved to more homogeneous compositions approaching the end-member muscovite. The effect of tectonic strain was fundamental both in the development of a metamorphic texture and the approach to chemical equilibrium.

*Keywords:* illite, anchizone-epizone, tectonic strain, slaty cleavage, electron microscopy.

## 1. Introduction

Illite occurs within argillaceous sedimentary rocks and is the most abundant clay mineral of the Earth's crust. Its composition is difficult to determine precisely because illite samples are usually physical mixtures of non-expanding 10-Å material and predominantly illitic, ordered mixed-layer illite/smectite. Values of 0.75–0.8 fixed K per $O_{10}(OH)_2$ at 0% expandability for illite/smectite have been reported by Hower and Mowatt (1966), Weaver (1965), Inoue and Utada (1983), Środoń et al. (1986), and Cuadros and Altaner (1998), among others. Illite is replaced by muscovite as a continuous restructuring process within greenschist and higher-grade metasedimentary rocks (Hunziker et al., 1986). Considerable mineralogical information has been produced for both illite and muscovite (for a review see Guidotti and Sassi, 1998). Nevertheless, relatively little is known about the specific mineralogical and chemical changes involved in the conversion of illite to muscovite within very low-grade metamorphic slates and about the importance of these chemical processes in the development of slaty cleavage fabric, where phyllosilicates are active participants.

Slaty cleavage is one of the main characteristics of regional metamorphism imparted to phyllosilicate-rich rocks and its development has been much debated for nearly 150 years (e.g. Sorby, 1853; Wood, 1974; White and Knipe, 1978; Lee et al., 1986; Wintsch et al., 1991; Van der Pluijm et al., 1998). Slaty cleavage is present in virtually all pelitic and some arenaceous rocks in the greenschist facies, and therefore appear at lower grades. Some authors have proposed that mechanical rotation of phyllosilicates in the earlier stages, probably accompanied by grain-boundary sliding and dissolution/neocrystallization ("pressure solution") are end-member processes that may be active during cleavage formation (Weber, 1981; Knipe, 1981; Ho et al., 1995, 1996). Pressure solution is an important deformation mechanism in sedimenta-

[1] Departamento de Geología, Universidad de Jaén, 23071 Jaén, Spain. <miabad@ujaen.es>
[2] Instituto Andaluz de Ciencias de la Tierra y Departamento de Mineralogía y Petrología, Universidad de Granada, 18002 Granada, Spain.
[3] Departamento de Geología, Universidad de Salamanca. 37008 Salamanca, Spain.

0036-7699/2003/83/63 

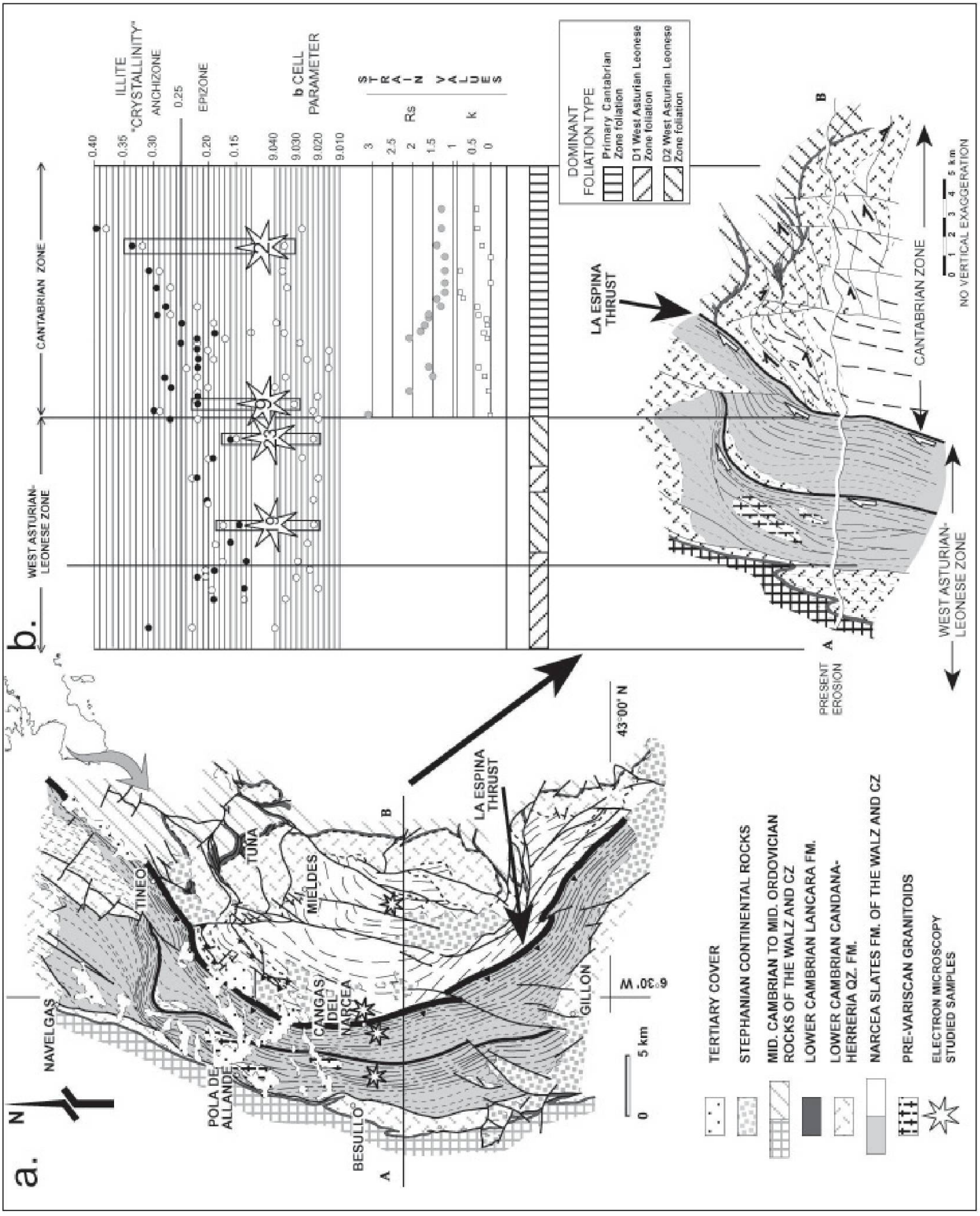
a.
N
NAVELGAS
TINEO
POLA DE ALLANDE
TUNA
MIELES
CANGAS DEL NARCEA
BESULLO
GILLON
LA ESPINA THRUST
A
B
6°30' W
43°00' N
0
5 km
TERTIARY COVER
STEPHANIAN CONTINENTAL ROCKS
MID. CAMBRIAN TO MID. ORDOVICIAN ROCKS OF THE WALZ AND CZ
LOWER CAMBRIAN LANCARA FM.
LOWER CAMBRIAN CANDANA-HERRERIA QZ. FM.
NARCEA SLATES FM. OF THE WALZ AND CZ
PRE-VARISCAN GRANITOIDS
ELECTRON MICROSCOPY STUDIED SAMPLES
b.
WEST ASTURIAN-LEONESE ZONE
CANTABRIAN ZONE
ILLITE "CRYSTALLINITY"
ANCHIZONE
EPIZONE
0.40
0.35
0.30
0.25
0.20
0.15
b CELL PARAMETER
9.040
9.030
9.020
9.010
STRAIN VALUES
Rs
k
3
2.5
2
1.5
1
0.5
0
DOMINANT FOLIATION TYPE
Primary Cantabrian Zone foliation
D1 West Asturian Leonese Zone foliation
D2 West Asturian Leonese Zone foliation
LA ESPINA THRUST
PRESENT EROSION
CANTABRIAN ZONE
WEST ASTURIAN-LEONESE ZONE
0 1 2 3 4 5 km
NO VERTICAL EXAGGERATION

*Fig. 1*

ry and metamorphic rocks (Kerrich, 1977), but it may also have important chemical and mineralogical consequences. The strain-induced dissolution of earlier phyllosilicates and the precipitation of new phyllosilicate grains are also both important processes in slaty cleavage development (Wintsch et al., 1991). In either case, the growth of micas has been shown to take place preferentially along cleavage domains (Weber, 1981; Knipe and White, 1977; Knipe, 1981) producing sharper illite XRD reflections that contribute to lower illite crystallinity values (Kübler, 1968). Knipe (1981) and Sutton (1989) even distinguished two kinds of domains in slates: P-domains, thin mica rich-zones, and Q-domains, quartz-rich regions, detecting differences in the average compositions of the micas from these two domains.

The aim of this paper is to describe the main textural and chemical features and changes between the slates which belong to the external and internal zones of a collisional orogen, the Variscan belt, using electron microscopy techniques (scanning and transmission). These techniques allow us to document by chemical analyses, backscattered electron images and lattice-fringe images, the changes in the population of white mica and chlorite crystallites of samples in response to prograde metamorphism and cleavage development. The results presented here will thus provide a better understanding of the chemical changes illite undergoes during incipient metamorphism. Lee et al. (1986) observed an increase in K and Al from bedding-parallel to cleavage-parallel illites and López-Munguira and Nieto (2000) found a change from illitic to muscovitic compositions coincident with the anchizone to epizone transition. However, in both cases the grain size of the samples allowed only AEM analyses, whereas high-quality *in-situ* analyses of coexistent illites and muscovites, such as those presented in this paper, were not possible.

## 2. Geology and materials

The very low to low-grade metamorphism transition in the Variscan belt of NW Spain (Fig. 1) is located across the boundary between the Cantabrian Zone (foreland, external domain), and the West Asturian-Leonese Zone (hinterland, internal domain) and it is marked by the presence of a structurally complex stack called the Narcea Antiform (Julivert, 1971; Gutiérrez-Alonso, 1996). This antiformal structure, which crops out in the Cantabrian Mountains, is exposed in a curved shape for a distance of more than 100 km. It is composed of terrigenous sedimentary rocks with turbiditic facies of the Upper Proterozoic Narcea Slates, unconformably overlain by shallow-water Cambrian–Ordovician deposits.

Both domains show major structural differences (Fig. 1a) and are separated by the La Espina thrust (Gutiérrez-Alonso, 1996). To the east, the Cantabrian Zone (CZ) was influenced by a single ductile deformation event imparting axial planar cleavage, mostly pressure solution seams, to the vertical axis folds recognized as related to strain partitioning at the root zone of the foreland and fold-thrust belt (Gutiérrez-Alonso, 1996). Overthrusting the Cantabrian Zone, the western domain of the Narcea thrust corresponds to the West Asturian-Leonese Zone (WALZ) where at least three superimposed ductile deformation events have been described (Gutiérrez-Alonso, 1996), the second being the most relevant one. The aforementioned second deformation event caused the kilometer-scale thrusting with strong E–W deformation gradients and the widespread formation of phyllonitic rock cleavage. This domain marks the boundary with the internal zones of the Variscan Belt in northwestern Spain.

The Narcea Antiform has been the subject of previous studies, such as the X-ray study of Gutiérrez-Alonso and Nieto (1996), which provided useful data for selection of the samples for this research. They reported the evolution of white-mica "crystallinity", **b** cell-parameter and mica basal spacing across this large structure and compared them with finite strain values and the intensity of cleavage development. All the relevant results related to white-mica XRD analysis are summarized in Fig. 1b.

Metamorphic conditions during the entire geological history of these rocks did not exceed the greenschist facies. The three recognized tectono-metamorphic events that took place in the western limb of the Narcea Antiform, causing the presence of a $D_1$ fold related cleavage and a $D_2$ shear related one, are related to the Variscan orogeny and occurred at 336 ± 0.3; and 321 ± 1 Ma, respectively (Dallmeyer et al., 1997); the third event is local and the sampling avoided sectors where it was present. The mineral assemblage established by XRD for the cross-section (Gutiér-

← *Fig. 1* (a) Geological and sample map of the Narcea antiform showing sampling points (compiled from Gutiérrez-Alonso, 1996); (b) results of white-mica XRD crystal-chemistry, strain analyses and dominant foliation types, plotted along the cross-section of the Narcea antiform (compiled from Gutiérrez-Alonso and Nieto, 1996).

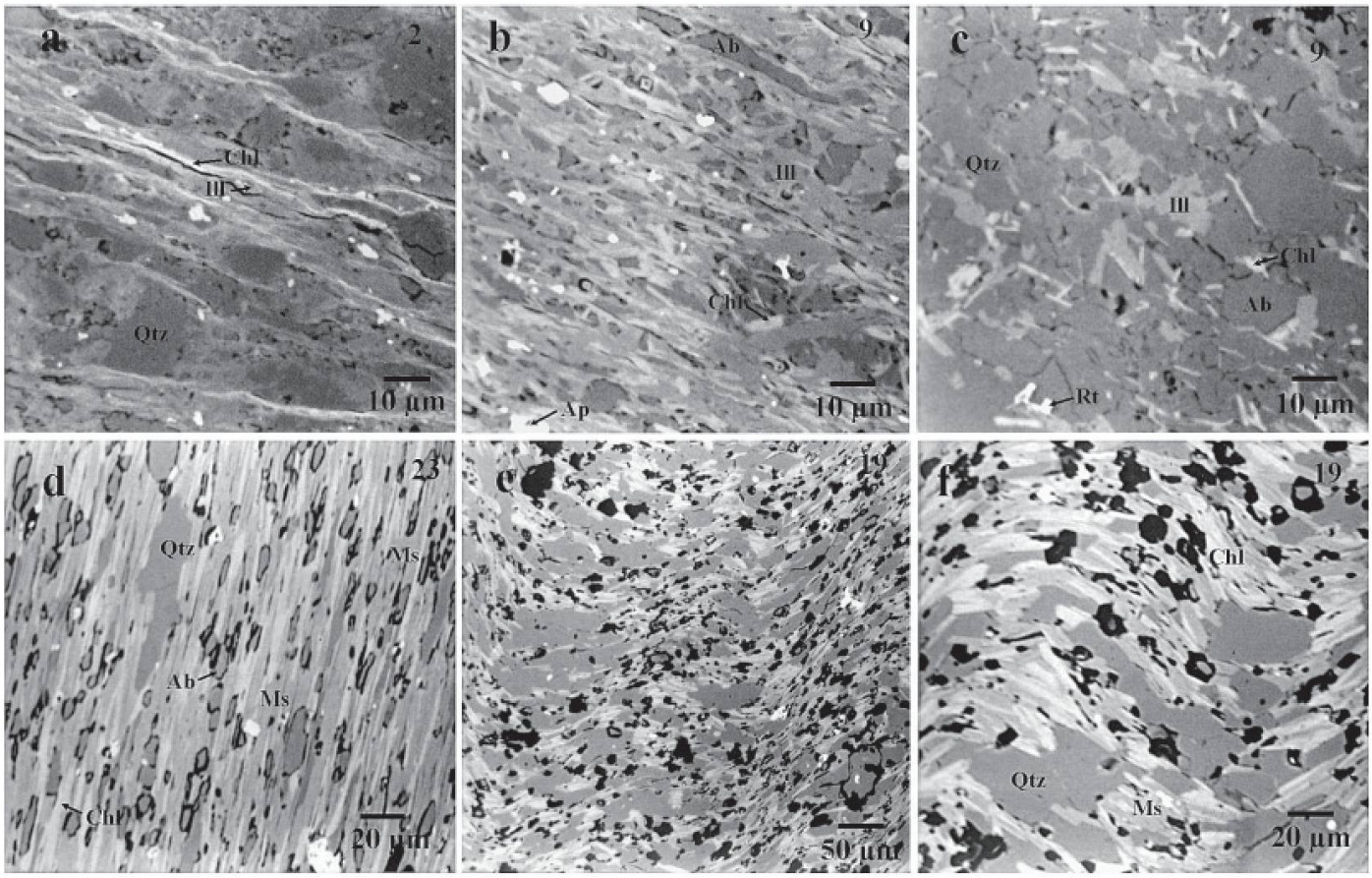


*Fig. 2* Back-scattered electron images showing texture of the slates. (a) Chlorite and mica fibres around anhedral quartz grains; (b and c) textural details of the light and dark bands characterizing sample 9, abundant in phyllosilicates and clearly quartzose, respectively; (d) well-developed schistosity in sample 23; metamorphic deformation is obvious; (e and f) texture of sample 19, with marked crenulation cleavage favouring the concentration of quartz in the hinges and of mica and chlorite in the limbs of the microfolds.

rez-Alonso and Nieto, 1996) is quartz + muscovite + chlorite ± albite. Moreover, rutile and Fe-oxides as accessory minerals have been recognized by SEM. In the CZ, large detrital white micas were observed, as well as small metamorphic ones, arranged parallel to the foliation. The origin of the detrital mica is complex and can be related to multiple orogenic events as deduced from the provenance studies performed in these rocks (Fernández-Suárez et al., 2000). In the WALZ, white mica is more abundant, crystals are larger and detrital grains are sparse.

As the Narcea Slates crop out in both zones, they are very adequated in order to compare the textural and chemical changes under very low grade metamorphism in both domains of the Variscan Belt.

Samples 2 (anchizone) and 9 (epizone) from CZ and 19 and 23 (both epizone) from WALZ (same numbering as in Gutiérrez-Alonso and Nieto, 1996) were selected (Fig. 1b) and prepared for electron microscopy studies. Samples 19 and 23 were selected as representative of those showing or lacking a secondary crenulation foliation (see Fig. 2).

The four samples are Upper Proterozoic Narcea Slates. The crystal-chemical parameters established by Gutiérrez-Alonso and Nieto (1996) were for sample 2: IC = 0.34 $\Delta°2\theta$ and **b** = 9.036 Å, for sample 9: IC = 0.22 $\Delta°2\theta$ and **b** = 9.031 Å and, for both samples 19 and 23: IC = 0.15 $\Delta°2\theta$ and **b** = 9.023 Å. The CZ data of the **b** parameter indicate intermediate pressure conditions according to Guidotti and Sassi (1986). The <2 μm fraction

*Table 1* Whole-rock analyses of major elements (oxide weight%).

| Samples | $SiO_2$ | $Al_2O_3$ | $Fe_2O_3$ | FeO | MnO | MgO | CaO | $Na_2O$ | $K_2O$ | $TiO_2$ | $P_2O_5$ | L.O.I. |
|---|---|---|---|---|---|---|---|---|---|---|---|---|
| 2 | 57.99 | 19.59 | 5.94 | 2.37 | 0.09 | 2.60 | 0.11 | 1.35 | 3.78 | 1.01 | 0.27 | 5.06 |
| 9 | 57.32 | 18.71 | 2.77 | 5.03 | 0.07 | 3.39 | 0.39 | 1.62 | 3.89 | 1.03 | 0.25 | 4.10 |
| 19 | 52.78 | 21.25 | 4.95 | 4.25 | 0.10 | 3.40 | 0.00 | 0.26 | 3.88 | 1.11 | 0.17 | 6.27 |
| 23 | 60.72 | 18.86 | 2.30 | 3.47 | 0.06 | 2.97 | 0.24 | 1.36 | 4.06 | 0.71 | 0.18 | 3.84 |

gives higher IC values (black spots in Fig. 1c) than the whole rock (open circles) and the **b** parameter is highly variable, both factors indicating the influence of detrital mica. The WALZ data indicate epizonal conditions and similar intermediate pressure conditions as in the CZ. In the case of WALZ data however, the <2 μm fraction gives IC values nearer to those of the whole rock and the **b** parameter is homogeneous, revealing that there is no influence of detrital white mica and that white mica is reequilibrated in these intermediate pressure conditions (Gutiérrez-Alonso and Nieto, 1996).

## 3. Methods

On the basis of the X-ray study of Gutiérrez-Alonso and Nieto (1996) four samples were selected as representative of the cross-section for a research by electron microscopy techniques. After the study by optical microscopy of thin sections oriented approximately perpendicular to the dominant planar fabric, carbon-coated samples were examined by Scanning Electron Microscopy (SEM), using back-scattered electron (BSE) imaging and energy-dispersive X-ray (EDX) analysis to obtain textural and chemical information and thinned ion-milled grids were studied by Transmission Electron Microscopy (TEM) at lattice scale. One of the samples has also been analyzed by Electron Microprobe (EMPA).

The electron microscopies employed for this research and the calculation of the structural formulae of the micas are the same as those described by Abad et al. (2002).

Microprobe analyses of white K-micas were performed using wavelength-dispersive spectroscopy (WDX) on a Cameca SX50 electron microprobe (EMPA) at the C.I.C. The instrument was set at an accelerating voltage of 20 kV, with a beam current of 30 nA and a beam diameter of <5 μm. Data were reduced using the procedure of Pouchou and Pichoir (1985) and the standards used were albite, orthoclase, periclase, wollastonite and synthetic oxides ($Al_2O_3$, $Fe_2O_3$ and $MnTiO_3$).

Due to the very fine-grained nature of these samples, the results obtained using the SEM and EMPA must sometimes be discarded due to varying degrees of contamination. It was necessary, therefore, to carry out a precise and meticulous selection of the portion of a grain to be analyzed using BSE images in the Z-contrast mode to improve the quality of the mica and chlorite analyses. When mica contamination is slight, the chlorite formula has been recalculated after subtracting for the contamination (determined from the K and/or Na content) from the initial analytical result using the remaining quantity of elements to fit a new formula, based on 28 negative charges (Nieto, 1997). Quantitative analyses (AEM) were obtained only from thin edges, using a (1000 × 200) Å scanning area as described by Abad et al. (2002).

Whole-rock analyses of the major elements were carried out using X-ray fluorescence (XRF) following Abad et al. (2002).

## 4. Results

### *4.1. Chemical bulk composition*

Chemical analyses of the major elements of the samples reveal homogeneous compositions, shown in Table 1. The data produce average values very similar to upper continental crust and average post-Archean Australian Shales (Taylor and McLennan, 1985). The Na content is slightly lower for sample 19 and the P contents are slightly higher in samples 2 and 9.

### *4.2. SEM observations*

BSE images of sample **2** (anchizone, CZ) illustrate that it has a fine-grained matrix and homogeneous texture. Mica and chlorite crystals often show anastomosing and curved intergrowths nearly parallel to bedding (Fig. 2a). The width of these phyllosilicate aggregates is less than several microns. In sample **9** (epizone, CZ) a light-dark banding is obvious at the millimeter-scale, the light bands (Fig. 2b) being richer in phyllosilicates (micas and chlorites) than the dark ones (Fig. 2c), which are rich in anhedral quartz grains and albite crystals.

Regarding the samples **19** and **23** (both epizone, WALZ), they show very similar textural features. In both of them the $D_2$ Variscan deformation episode is responsible for the main $S_2$ foliation observed (Fig. 2d). In addition, the crenulation $S_2$' in sample 19 (Figs. 2e–f) is the result of a progressive shear state caused by thrusts that developed during the $D_2$ episode (Gutiérrez-Alonso, 1992).

BSE images show clear differences in texture between the two groups of samples. The rocks from the CZ reveal bedding-parallel phyllosilicate preferred orientations while axial planar cleavage is mostly caused by pressure solution processes, whereas the WALZ slates are characterized by cleavage-parallel or -subparallel mica

*Table 2* EMPA, SEM and AEM data for micas in sample 23.

| Representative electron-microprobe analyses (wt%) | | | | | | | | |
|---|---|---|---|---|---|---|---|---|
| analyses | $SiO_2$ | $Al_2O_3$ | MgO | FeO | $TiO_2$ | $Na_2O$ | $K_2O$ | Total |
| 23 z2 8 | 17.62 | 14.24 | 1.20 | 0.82 | 0.10 | 0.19 | 4.58 | 93.43 |
| 23 z2 11 | 17.75 | 14.07 | 1.27 | 0.82 | 0.08 | 0.16 | 4.57 | 94.65 |
| 23 z2 13 | 17.77 | 14.03 | 1.24 | 0.78 | 0.10 | 0.14 | 4.68 | 94.33 |
| 23 z2 14 | 17.71 | 14.08 | 1.13 | 0.89 | 0.10 | 0.17 | 4.68 | 93.44 |
| 23 z2 15 | 17.84 | 14.15 | 1.08 | 0.71 | 0.09 | 0.16 | 4.67 | 91.71 |

| Structural formulae normalized to $O_{10}(OH)_2$ | | | | | | | | | | |
|---|---|---|---|---|---|---|---|---|---|---|
| | Si | $^{IV}Al$ | $^{VI}Al$ | Fe | Mg | Ti | $^{VI}\Sigma$ | K | Na | $\Sigma$ inter. |
| **EMPA** | | | | | | | | | | |
| 23 z2 8 | 3.15 | 0.85 | 1.70 | 0.15 | 0.21 | 0.02 | 2.08 | 0.82 | 0.03 | 0.85 |
| 23 z2 11 | 3.17 | 0.83 | 1.69 | 0.15 | 0.23 | 0.01 | 2.08 | 0.82 | 0.03 | 0.85 |
| 23 z2 13 | 3.18 | 0.82 | 1.69 | 0.14 | 0.22 | 0.02 | 2.07 | 0.84 | 0.03 | 0.86 |
| 23 z2 14 | 3.17 | 0.83 | 1.69 | 0.16 | 0.20 | 0.02 | 2.06 | 0.84 | 0.03 | 0.87 |
| 23 z2 15 | 3.19 | 0.81 | 1.72 | 0.13 | 0.19 | 0.02 | 2.05 | 0.83 | 0.03 | 0.86 |
| **SEM** | | | | | | | | | | |
| 23–1 | 3.20 | 0.80 | 1.68 | 0.17 | 0.18 | 0.02 | 2.05 | 0.84 | 0.00 | 0.84 |
| 23–2 | 3.22 | 0.78 | 1.58 | 0.20 | 0.25 | 0.02 | 2.04 | 0.90 | 0.03 | 0.93 |
| 23–3 | 3.24 | 0.76 | 1.61 | 0.18 | 0.23 | 0.02 | 2.04 | 0.85 | 0.04 | 0.89 |
| 23–5 | 3.24 | 0.76 | 1.64 | 0.15 | 0.20 | 0.02 | 2.02 | 0.90 | 0.03 | 0.93 |
| **AEM** | | | | | | | | | | |
| 23–3r | 3.07 | 0.93 | 1.61 | 0.18 | 0.27 | 0.02 | 2.09 | 0.91 | 0.04 | 0.95 |
| 23–4r | 3.12 | 0.88 | 1.65 | 0.14 | 0.26 | 0.02 | 2.08 | 0.93 | 0.01 | 0.94 |
| 23–7r | 3.05 | 0.95 | 1.60 | 0.17 | 0.29 | 0.03 | 2.09 | 0.96 | 0.03 | 1.00 |
| 23–8r | 3.04 | 0.96 | 1.56 | 0.22 | 0.31 | 0.03 | 2.11 | 0.95 | 0.02 | 0.97 |
| 23–11r | 3.08 | 0.92 | 1.60 | 0.18 | 0.28 | 0.02 | 2.08 | 0.94 | 0.04 | 0.98 |

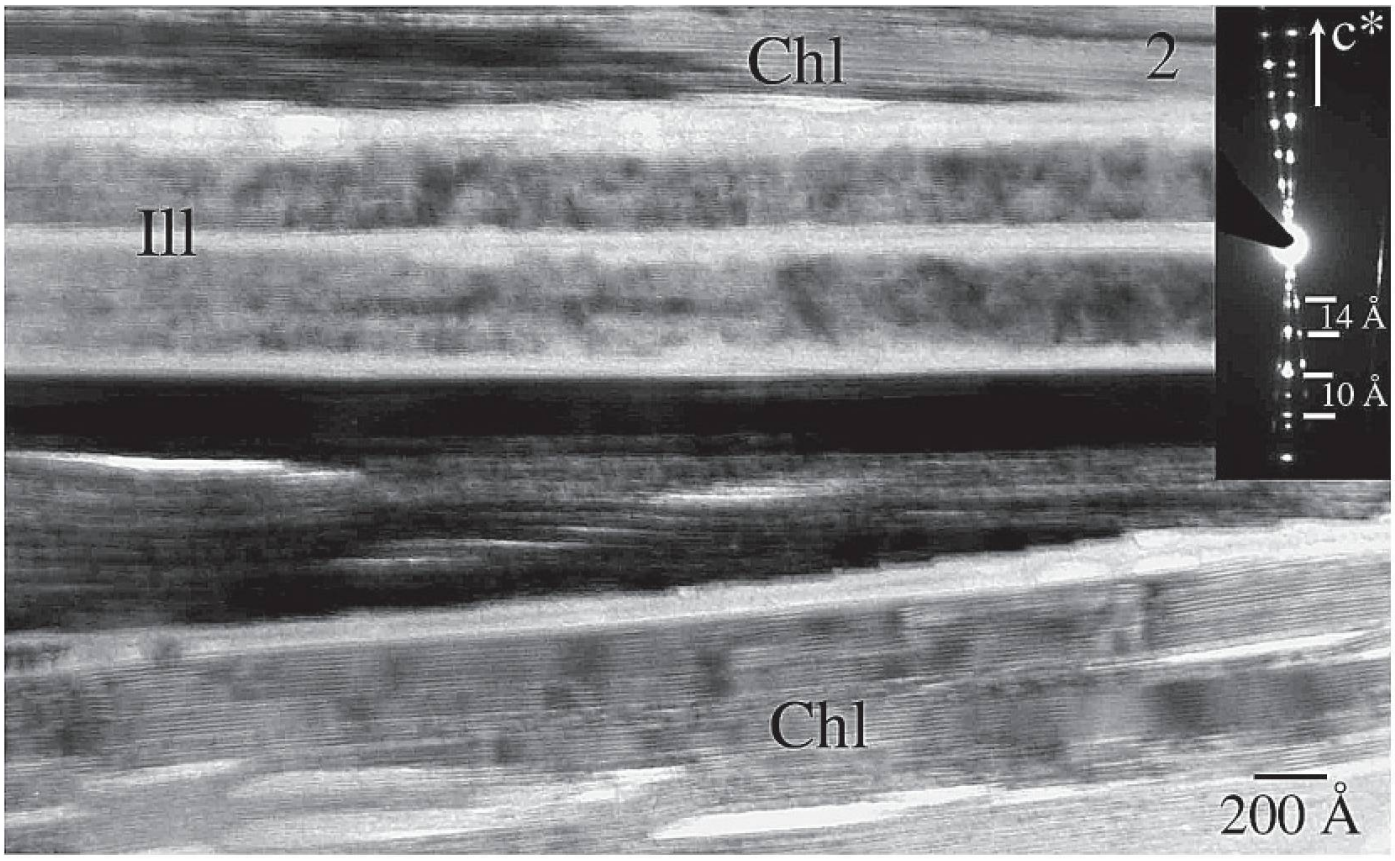


*Fig. 3* Chlorite packets with lenticular fissures and microfolds with an illite packet in a subparallel orientation between them. The SAED reveals the reflections of both phases and a slight, low-angle contact among the different packets.

and chlorite preferred orientations. The fabric of the WALZ samples shows the effects of strain whereas the CZ mica fabric is inherited from sedimentary or diagenetic processes.

### *4.3. TEM observations*

This research presents results based on 48 lattice fringe images and 26 selected area electron diffraction (SAED) patterns.

Sample **2** gives lattice-fringe images of illite crystals with 10-Å and 20-Å periodicities; the latter is the result of dynamic effects and confirms the 2M polytype determined by the SAED patterns. The illitic grains are well-defined 200- to 500-Å thick packets and lie parallel to chlorite packets (Fig. 3). The chlorite crystals are thicker and commonly show lenticular voids and wavy, folded layers (Fig. 3). Periodicities of 28, 42 and 56 Å have been detected in the lattice images of chlorite packets (Fig. 4), as well as 7-Å individual layers.

Chlorite packets also show 24-Å periodicities (Fig. 5), due to the random presence of 10-Å individual layers. AEM data for these areas show a lower octahedral sum of cations than usual in chlorites (see Table 4) and no correlation exists between these data and a possible content of interlayer cations, such as K and Na, due to smectite and/or mica contamination. A review of the XRD diagrams of Gutiérrez-Alonso and Nieto (1996) for the <2 μm fraction has revealed that no change was produced after ethylen-glycol treatment and the sample heated to 550 °C produced a 12.1 Å peak, interpreted as the second-order peak of a 24.24 Å reflection, that is, a random mixed-layer composed of 14 Å (chlorite) and 10 Å (contracted vermiculite) (Banfield and Murakami, 1998).

As expected from its lower IC value, in sample **9** mica and chlorite crystals are thicker than in sample 2. Defects are uncommon, except layer terminations, and voids. A notable feature is that crystals usually form high-angle grain-boundaries (Fig. 6).

Lattice images from samples **19** and **23** (WALZ) show large (>1000 Å in thickness), defect-free 2M polytype muscovite crystals (Fig. 7, inset), with a mottled texture and elongated nar-

*Table 3* Structural formulae* for micas in samples 2, 9 and 19 on the basis of SEM data.

| Samples | Si | $^{IV}$Al | $^{VI}$Al | Fe | Mg | Ti | $^{VI}\Sigma$ | K | Na | Σ inter. |
|---|---|---|---|---|---|---|---|---|---|---|
| 2–4 | 3.40 | 0.60 | 1.63 | 0.20 | 0.18 | 0.01 | 2.02 | 0.76 | 0.00 | 0.76 |
| 2–5 | 3.64 | 0.36 | 1.70 | 0.09 | 0.17 | 0.01 | 1.97 | 0.63 | 0.00 | 0.63 |
| 2–6 | 3.29 | 0.71 | 1.76 | 0.12 | 0.16 | 0.01 | 2.06 | 0.66 | 0.05 | 0.72 |
| 2–7 | 3.20 | 0.80 | 1.56 | 0.26 | 0.15 | 0.04 | 2.01 | 0.91 | 0.03 | 0.94 |
| 2–8 | 3.15 | 0.85 | 1.52 | 0.28 | 0.19 | 0.04 | 2.04 | 0.90 | 0.05 | 0.95 |
| 2–9 | 3.22 | 0.78 | 1.62 | 0.23 | 0.21 | 0.02 | 2.07 | 0.75 | 0.06 | 0.81 |
| 2–10 | 3.33 | 0.67 | 1.62 | 0.25 | 0.16 | 0.01 | 2.05 | 0.70 | 0.04 | 0.74 |
| 2–12 | 3.54 | 0.46 | 1.45 | 0.32 | 0.26 | 0.02 | 2.06 | 0.60 | 0.00 | 0.60 |
| 9–1 | 3.65 | 0.35 | 1.48 | 0.32 | 0.19 | 0.01 | 2.00 | 0.56 | 0.04 | 0.60 |
| 9–2 | 3.50 | 0.50 | 1.52 | 0.24 | 0.23 | 0.02 | 2.01 | 0.75 | 0.00 | 0.75 |
| 9–4 | 3.32 | 0.68 | 1.68 | 0.15 | 0.15 | 0.02 | 1.99 | 0.84 | 0.03 | 0.87 |
| 9–5 | 3.43 | 0.57 | 1.56 | 0.18 | 0.25 | 0.01 | 2.01 | 0.78 | 0.06 | 0.83 |
| 9–6 | 3.56 | 0.44 | 1.66 | 0.11 | 0.15 | 0.02 | 1.94 | 0.77 | 0.00 | 0.77 |
| 9–8 | 3.32 | 0.68 | 1.65 | 0.17 | 0.18 | 0.02 | 2.02 | 0.75 | 0.07 | 0.82 |
| 9–9 | 3.34 | 0.66 | 1.63 | 0.12 | 0.23 | 0.01 | 2.00 | 0.92 | 0.00 | 0.92 |
| 9–10 | 3.26 | 0.74 | 1.53 | 0.23 | 0.29 | 0.02 | 2.08 | 0.84 | 0.00 | 0.84 |
| 9–11 | 3.33 | 0.67 | 1.56 | 0.17 | 0.27 | 0.01 | 2.00 | 0.94 | 0.03 | 0.97 |
| 9–12 | 3.37 | 0.63 | 1.61 | 0.15 | 0.21 | 0.02 | 1.98 | 0.90 | 0.00 | 0.90 |
| 9–13 | 3.33 | 0.67 | 1.68 | 0.15 | 0.18 | 0.02 | 2.03 | 0.78 | 0.00 | 0.78 |
| 9–15 | 3.32 | 0.68 | 1.53 | 0.19 | 0.23 | 0.06 | 2.01 | 0.87 | 0.00 | 0.87 |
| 19–2 | 3.21 | 0.79 | 1.58 | 0.25 | 0.21 | 0.03 | 2.06 | 0.83 | 0.03 | 0.86 |
| 19–3 | 3.23 | 0.77 | 1.63 | 0.19 | 0.18 | 0.02 | 2.02 | 0.87 | 0.04 | 0.91 |
| 19–4 | 3.23 | 0.77 | 1.65 | 0.19 | 0.20 | 0.02 | 2.06 | 0.81 | 0.00 | 0.81 |
| 19–9 | 3.27 | 0.73 | 1.61 | 0.19 | 0.22 | 0.02 | 2.04 | 0.86 | 0.00 | 0.86 |
| 19–11 | 3.26 | 0.74 | 1.63 | 0.18 | 0.18 | 0.02 | 2.00 | 0.88 | 0.05 | 0.94 |
| 19–13 | 3.26 | 0.74 | 1.61 | 0.22 | 0.20 | 0.02 | 2.05 | 0.83 | 0.00 | 0.83 |
| 19–14 | 3.23 | 0.77 | 1.59 | 0.22 | 0.23 | 0.02 | 2.06 | 0.86 | 0.00 | 0.86 |
| 19–15 | 3.26 | 0.74 | 1.64 | 0.18 | 0.19 | 0.02 | 2.03 | 0.87 | 0.00 | 0.87 |

* Normalized to $O_{10}(OH)_2$ and considering 75% of Fe as $Fe^{3+}$ and 25% as $Fe^{2+}$.

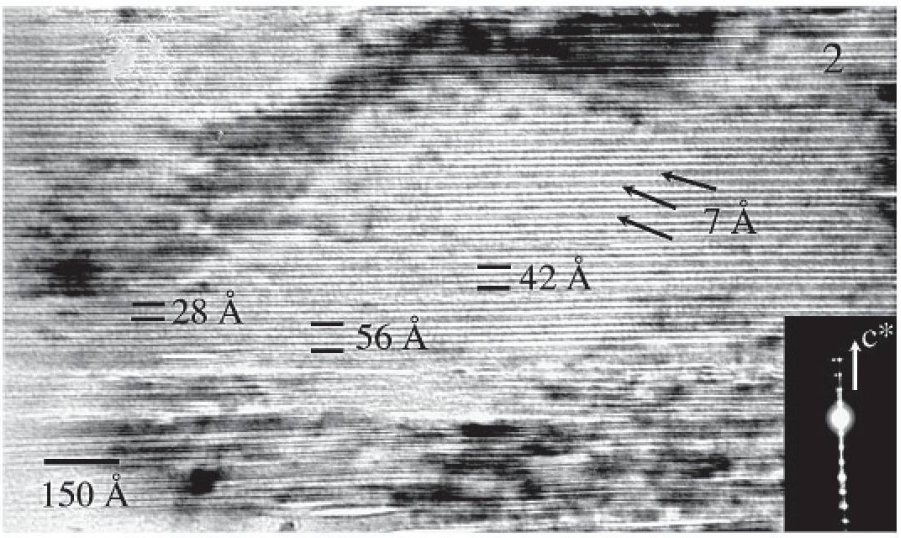


*Fig. 4* Lattice-fringe image of a chlorite with fissures, contrast changes and distinct layer periodicities at 14 Å with alternating individual layers at 7 Å. Under SAED, the basal diffractions show dynamic effects produced by complex, multilayered polytypes at 14 Å.

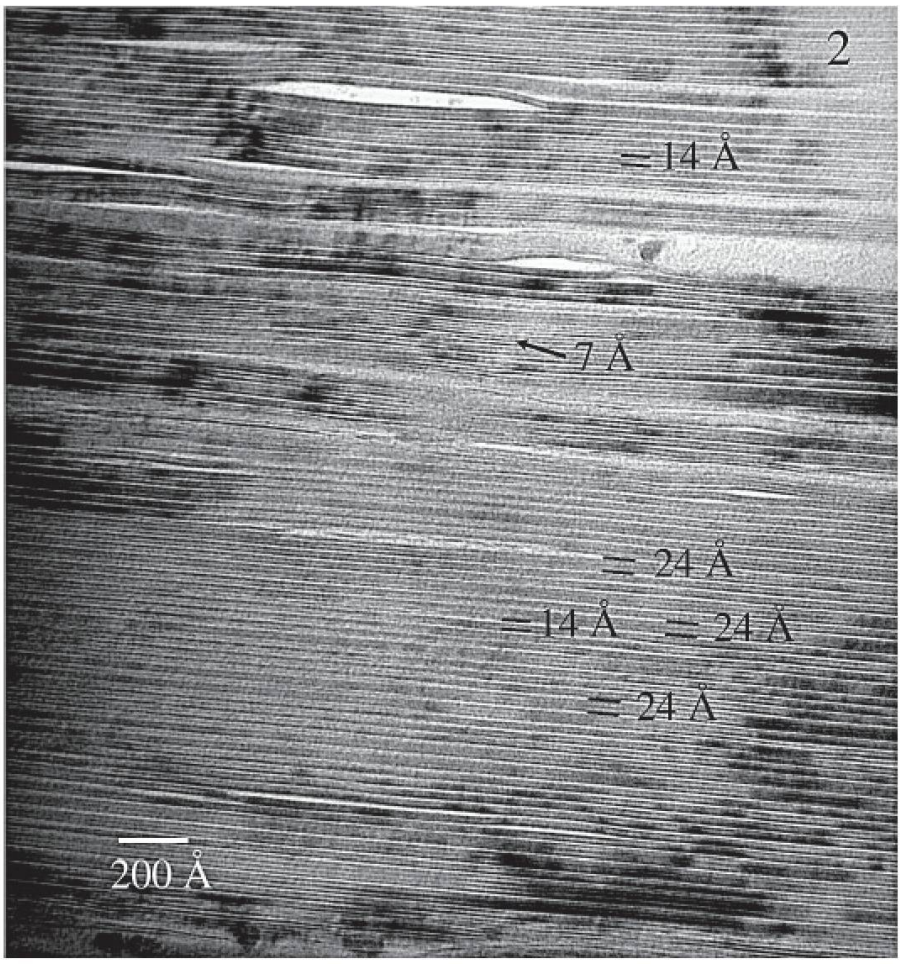


*Fig. 5* Lattice-fringe image of fissured chlorite and layers at 14 Å (black and white layer) alternating with layers at 24 Å (14 + 10, two black and one white). The microanalysis is low in octahedral elements (see Table 4).

row voids parallel to the layers (Fig. 7). Chlorite crystals are homogeneous and defect-free and sometimes show complex stacking sequences due to superperiodicities such as 56 Å (Fig. 8). Figure 9 shows microfolds and kinks that developed in a chlorite as a consequence of a late deformation episode ($S_2$'); this feature is similar to that described in the backscattered images (Figs. 2 e–f).

The lattice-fringe images of the anchizone sample reveal a serie of textural features (fissures, layer contrast, etc.) that indicate the first strains of incipient metamorphism (CZ). These same strains

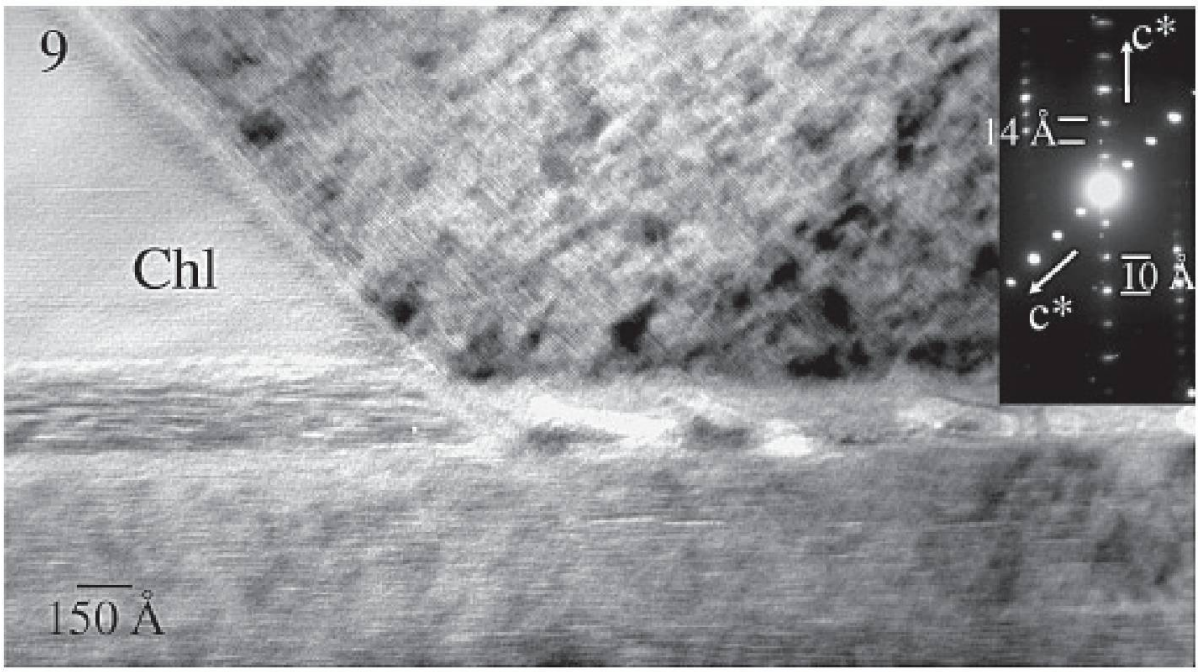


*Fig. 6* Lattice-fringe image showing the textural relationships between a chlorite crystal and two dioctahedral mica crystals, one with the same orientation as the chlorite and a periodicity at 20 Å and the other with an angle contact with the chlorite and a periodicity at 10 Å.

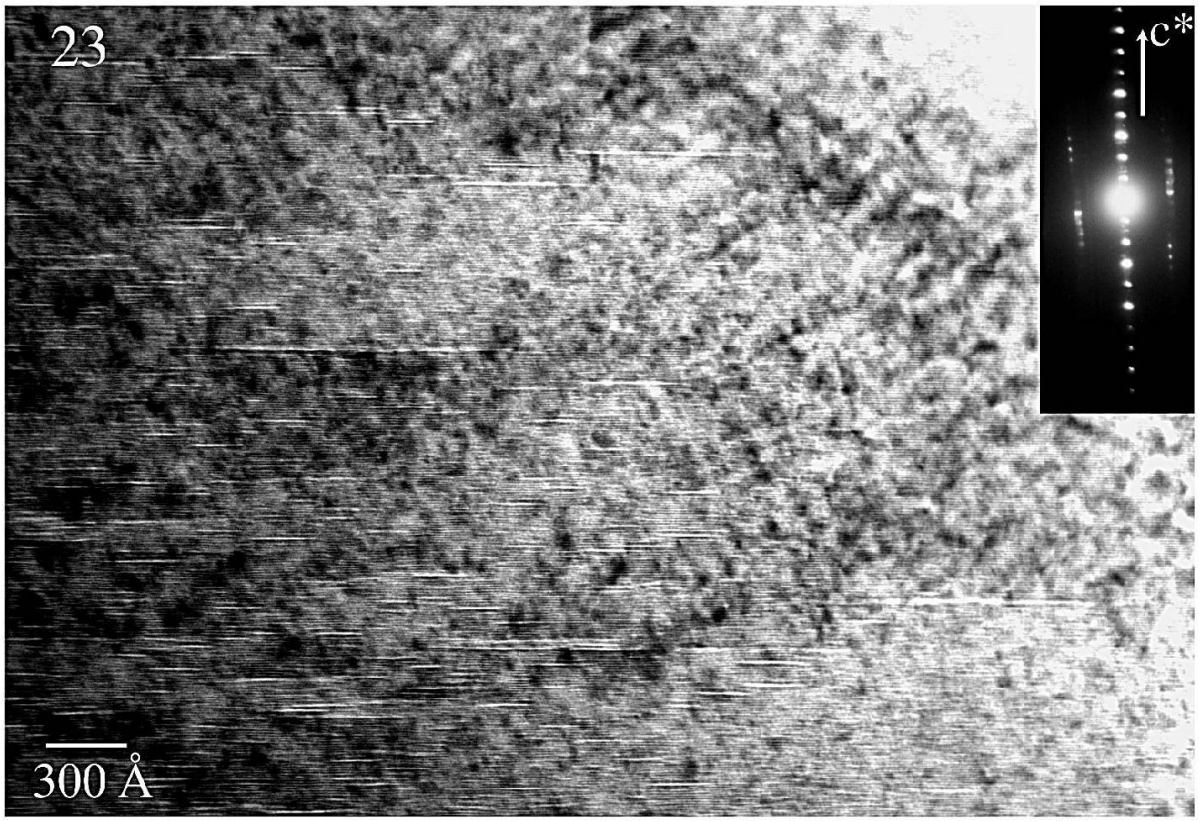


*Fig. 7* Lattice-fringe image of part of a 2M muscovite crystal with a thickness of over 5000 Å. This crystal is characterized by its mottled texture and the presence of narrow fissures.

later produce the cleavage and microfolds in rocks with a stronger deformation that are clearly metamorphic, such as epizone-grade conditions (WALZ). The texture of the latter is definitely different, with large, parallel defect-free packets of muscovite and chlorite (Figs. 7 and 8). Thus, the highly crystalline character is responsible for the low IC values ($\approx 0.15\ \Delta°2\theta$).

Chlorite shows more obviously some typical strain features than micas; both phyllosilicates form sub-parallel, low-angle intergrowths. The most common strain features in these samples

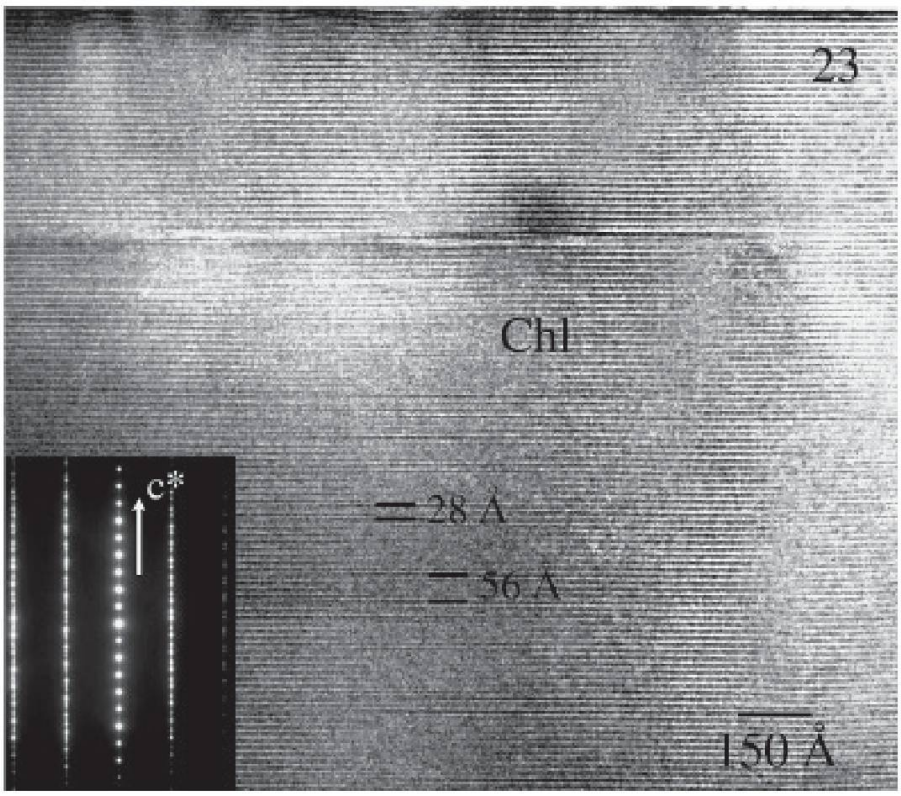


*Fig. 8* Two-dimensional lattice-fringe image showing part of a chlorite crystal more than 4000 Å thick. An ordered polytype can be seen in the SAED image. It is crystalline in appearance and very uniform. In some cases, the 14 Å layers are grouped two by two or four by four, apparently randomly.

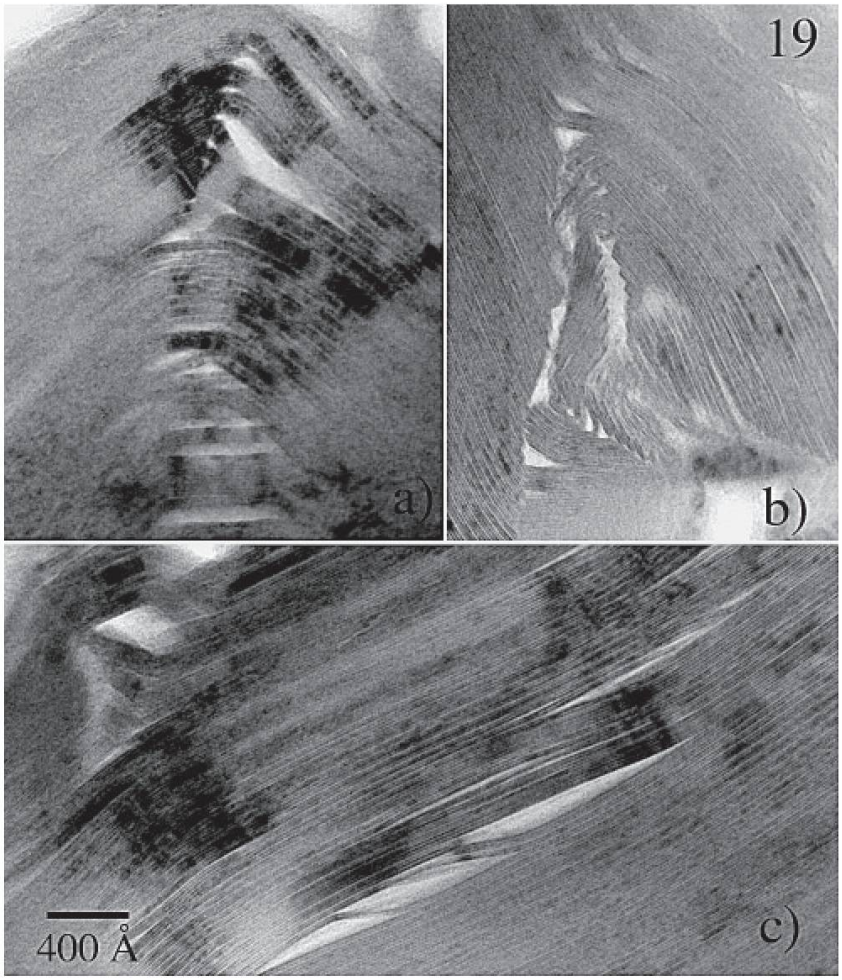


*Fig. 9* Textural features of chlorite: (a) microfolds, (b) chevron fold with slipping and detachment of layers, (c) box folds to the left and the development of cracks due to deformation.

are: (a) lenticular and narrow voids along slip surfaces (Figs. 4 and 5); (b) fringe contrasts oblique to the layers, generated by stress in the defects; and (c) polygonal microfolds (Fig. 9).

### *4.4. Chemical compositions of phyllosilicates*

Determination of the chemical composition of phyllosilicates in sub-greenschist facies rocks is severely limited because of their small grain size and defect-rich character. The spot size of EMPA resolution is usually too large and AEM produces lower-quality results and is severely affected by alkali loss. As a consequence, the chemical evolution of clay minerals from the diagenetic stage to low-grade metamorphism is still poorly known. As sample 23 has a large enough grain size to allow microprobe analysis, this sample was used to check the quality of the various analytical techniques.

#### *4.4.1. Dioctahedral micas*

Table 2 presents some representative analyses for micas of sample 23 obtained using SEM, EMPA and AEM techniques. Analyses obtained by EDX in the SEM have a similar compositional range to that obtained with EMPA, with the single exception of Al, which is slightly higher under EMPA. AEM analyses are affected by a higher error (3–12%) but are always in the expected precision range for this technique (around 10–15%). Mg is the most affected cation (25%), probably due to problems in the background fitting in the Al-peak slope region.

As all the samples show a suitable size for analysis by SEM and Table 2 reveals that this technique produces results of a similar quality to those obtained by EMPA, SEM has been employed to study the chemical composition of phyllosilicates in the Narcea samples.

Tables 2 and 3 show the chemical mica compositions of the four analyzed samples. The sum of the octahedral cations is in general only slightly higher than 2 atoms per formula unit (a.f.u.), which is an additional quality proof of the analyses. Ca and Mn are always under 0.01 a.f.u., and are therefore not shown in the Tables. Ti is present in all the analyses in significant proportions (0.01–0.06 a.f.u.). Na is either absent or present in small proportions ($\leq 0.07$ a.f.u.) and therefore paragonitic substitution is not significant in these samples. Albite is present as a metamorphic phase, which, in addition to the low-temperature conditions, must be responsible for both the lack of paragonite as a discrete phase and the scarcity of the paragonitic substitution in the K-micas.

The interpretation of the chemical composition of micas is complex because each chemical parameter is affected by several compositional vectors (Fig. 10). A negative correlation between interlayer population and Si can be explained by illitic substitution (Fig. 10a). Nevertheless, the analyses do not plot exactly on the theoretical trend due to the effect of phengitic substitution. Figure 10b shows the effect of the ferrimuscovitic vector. This ferrimuscovitic vector significantly affects the chemical variables represented in Figs. 10c and 10d, which show a phengitic tendency. This is the main vector determining the proportions of Si, Al and Fe + Mg, but these chemical parameters are also affected by the ferrimuscovitic and illitic vectors.

The most evident characteristic of all these diagrams is the scattered character of the CZ analyses in relation to those of the WALZ. In general, the CZ compositions extend over a wide range that includes the narrower field of chemical variations corresponding to the WALZ samples. This field is located in the nearest position to the theoretical muscovite in Figs. 10 a-c-d and in the central position of Fig. 10b. In other words, the WALZ micas have attained greater homogeneity in relation to those of the CZ which tend towards higher phengite and illite contents (sum of interlaminar cations = 0.60–0.97 a.f.u. in the CZ vs. 0.81–0.93 a.f.u. in the WALZ). No significant differences can be detected between samples from the same geological zone (Fig. 10).

As regards the $Fe^{3+}$ content, Fig. 10b shows that there is no correlation with metamorphic evolution, with the exception of the homogenization trend towards higher grades. Therefore, the $Fe^{3+}/Fe^{2+}$ rate must be essentially a function of the redox conditions, as Guidotti et al. (1994) proposed.

The evaluation of the analysis quality would seem to indicate that, as the grain size is smaller in the CZ samples, they might be more affected by problems of contamination. However, the trends shown in the diagrams can be satisfactorily explained in the light of three exchange vectors (Fig. 10) that are incompatible assuming a contamination by other mineral phases, particularly chlorite. Specifically, applied to white mica, chlorite would cause a drop in Si content related with a decrease in interlayer cations. Exactly the opposite tendency can be observed in Fig. 10a. Such a tendency would be accompanied also by an increase in the sum of octahedral cations, which is not seen in the CZ samples compared to those of the WALZ (Tables 2–3). A similar evaluation of the relationships between the various chemical parameters of the mica formulae has allowed us to discard the

*Table 4* EMPA, SEM and AEM data for chlorites.

| Electron-microprobe analyses (wt%) | | | | | | | | | |
|---|---|---|---|---|---|---|---|---|---|
| Samples | $SiO_2$ | $Al_2O_3$ | MgO | FeO | $MnO_2$ | $TiO_2$ | $Na_2O$ | $K_2O$ | Total |
| 23,1 | 11.69 | 11.40 | 9.13 | 8.72 | 0.10 | 0.03 | 0.05 | 0.22 | 88.1 |
| 23,2 | 11.63 | 10.98 | 9.55 | 8.81 | 0.09 | 0.14 | 0.18 | 0.02 | 83.9 |
| 23,3 | 11.16 | 11.09 | 9.88 | 9.29 | 0.11 | 0.04 | 0.00 | 0.04 | 86.6 |
| 23,4 | 11.27 | 11.13 | 9.82 | 9.12 | 0.11 | 0.04 | 0.01 | 0.06 | 86.56 |
| 23,5 | 11.18 | 11.19 | 9.73 | 9.23 | 0.11 | 0.06 | 0.03 | 0.05 | 86.22 |
| Structural formula normalized to $O_{10}(OH)_8$ | | | | | | | | | |
| | Si | $^{IV}Al$ | $^{VI}Al$ | Fe | Mg | Mn | Ti | $^{VI}\Sigma$ | Fe/Fe+Mg |
| **EMPA** | | | | | | | | | |
| 23,1 | 2.73 | 1.27 | 1.45 | 2.18 | 2.28 | 0.02 | 0.01 | 5.93 | 0.49 |
| 23,2 | 2.74 | 1.26 | 1.35 | 2.18 | 2.36 | 0.02 | 0.03 | 5.94 | 0.48 |
| 23,3 | 2.68 | 1.32 | 1.34 | 2.23 | 2.37 | 0.03 | 0.01 | 5.98 | 0.48 |
| 23,4 | 2.70 | 1.30 | 1.37 | 2.19 | 2.36 | 0.03 | 0.01 | 5.95 | 0.48 |
| 23,5 | 2.68 | 1.32 | 1.37 | 2.21 | 2.34 | 0.03 | 0.01 | 5.96 | 0.49 |
| **SEM** | | | | | | | | | |
| 23 1 | 2.76 | 1.24 | 1.34 | 2.33 | 2.25 | 0.04 | 0.00 | 5.95 | 0.51 |
| 23 3 | 2.79 | 1.21 | 1.31 | 2.35 | 2.25 | 0.03 | 0.02 | 5.97 | 0.51 |
| 23 4 | 2.78 | 1.22 | 1.35 | 2.32 | 2.24 | 0.03 | 0.00 | 5.94 | 0.51 |
| 19 1 | 2.90 | 1.10 | 1.62 | 2.29 | 1.79 | 0.03 | 0.01 | 5.74 | 0.56 |
| 19 2 | 2.82 | 1.18 | 1.54 | 2.40 | 1.86 | 0.03 | 0.00 | 5.84 | 0.56 |
| 19 3 | 2.78 | 1.22 | 1.49 | 2.45 | 1.89 | 0.03 | 0.00 | 5.87 | 0.56 |
| 9 3 | 2.68 | 1.32 | 1.29 | 2.75 | 1.99 | 0.03 | 0.00 | 6.06 | 0.58 |
| **AEM** | | | | | | | | | |
| 23 4 | 2.43 | 1.57 | 1.14 | 2.45 | 2.52 | 0.05 | 0.02 | 6.17 | 0.49 |
| 23 6 | 2.61 | 1.39 | 1.17 | 2.47 | 2.46 | 0.02 | 0.00 | 6.11 | 0.50 |
| 23 1 | 2.59 | 1.41 | 1.23 | 2.33 | 2.49 | 0.04 | 0.00 | 6.09 | 0.48 |
| 23 2 | 2.77 | 1.23 | 1.41 | 2.30 | 2.15 | 0.05 | 0.00 | 5.91 | 0.52 |
| *chlorite-rich mixed-layers (see text)* | | | | | | | | | |
| 2 1 | 3.00 | 1.00 | 1.84 | 2.22 | 1.48 | 0.03 | 0.00 | 5.58 | 0.60 |
| 2 2 | 2.83 | 1.17 | 1.60 | 2.51 | 1.66 | 0.02 | 0.00 | 5.78 | 0.60 |
| 2 3 | 3.05 | 0.95 | 1.74 | 2.16 | 1.71 | 0.00 | 0.00 | 5.61 | 0.56 |

possibility that illitic substitution in CZ samples was an artifact caused by the effect of the alkaline cation loss. In this case, the deficit of K+Na would not be clearly related with a Si increase, but would produce a general increase in the formulae of all the non-alkaline elements. This finally should cause a clear increase of the octahedral sum.

#### *4.4.2. Trioctahedral chlorite*

Table 4 shows the chemical compositions obtained using EMPA, SEM and AEM. Figure 11 shows nearly constant proportion of Al and a negative correlation between Si and Fe + Mg. The ratio of Fe/(Fe + Mg) in WALZ chlorites is very constant, with a range of 0.48–0.58, and the $^{VI}Al$ content is only slightly higher than the $^{IV}Al$ one and even lower in several cases.

Due to contamination by vermiculite layers (Fig. 5) or dioctahedral micas in chlorites from the CZ samples, these data could not be used to study possible chemical differences between the CZ and WALZ chlorites.

## 5. Discussion

### *5.1. Fabric evolution of the slates*

The two principal mechanisms that Ho et al. (1995, 1996) reviewed for the reorientation of phyllosilicates associated with cleavage formation are: (1) mechanical rotation of pre-existing grains, and (2) dissolution and neocrystallization ('pressure solution'). Mechanical rotation of grains would create a continuous range of different orientations between bedding parallel layering and

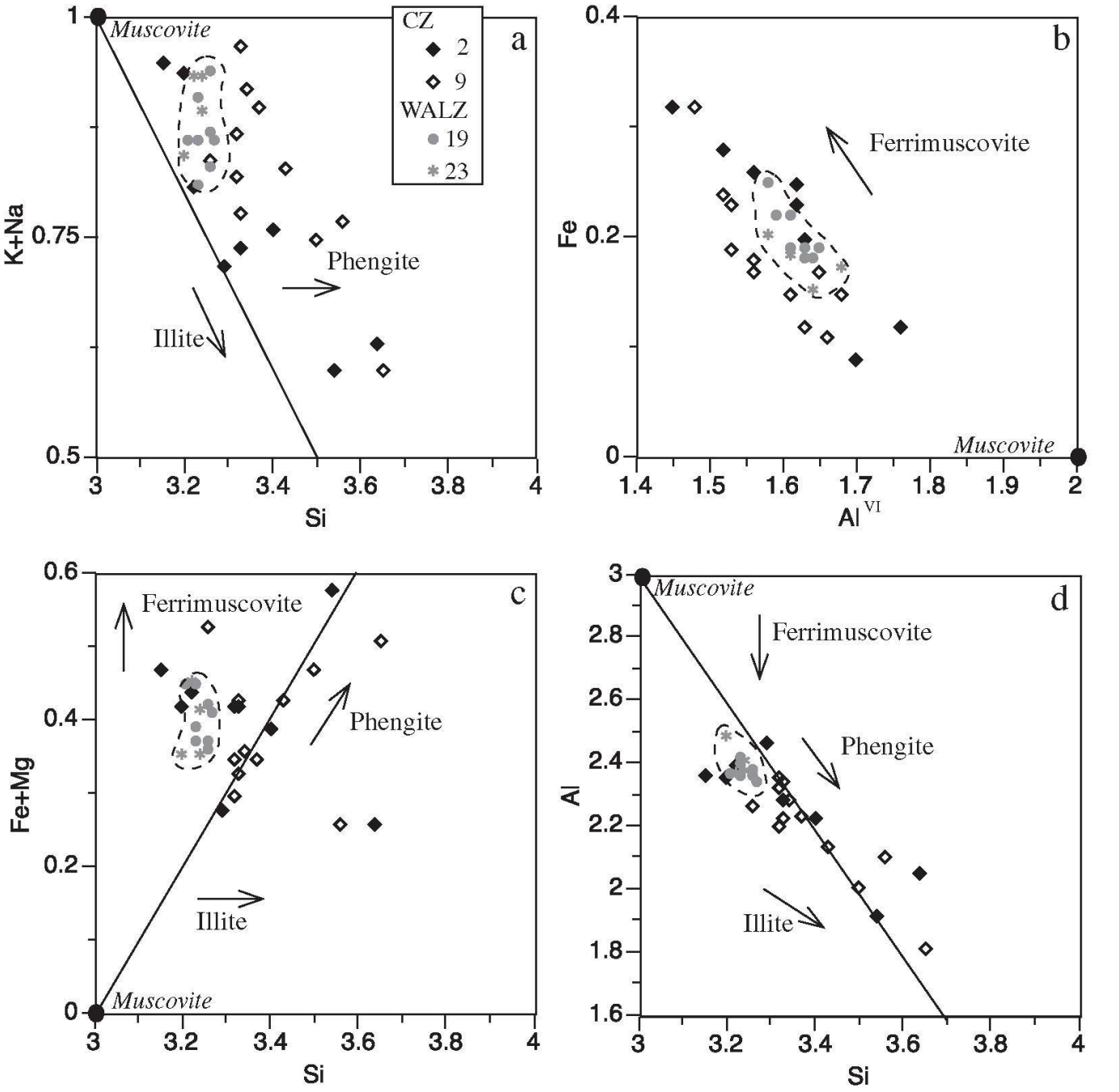


*Fig. 10* Diagrams of the chemical composition of micas of the samples from the Narcea Antiform. The grey symbols represent the WALZ samples (19 and 23) and the black symbols the CZ samples (2 and 9), the former with a higher metamorphic grade.

cleavage parallel reorientation, but in the Narcea samples transitional orientations are absent. According to Merriman and Peacor (1999), the formation of slaty cleavage microfabrics in the anchizone and epizone is a response to the combined effects of thermal and strain energy in the early stages of regional metamorphism. Van der Pluijm et al. (1998) have pointed out that the contribution of either source to the total energy of the system is interchangeable and complementary, favouring mechanical grain kinking and rotation processes in low-energy environments (CZ), and chemically-driven processes such as grain dissolution and neocrystallization in high-energy environments (WALZ). Cleavage surfaces are well developed in the WALZ samples and the fabric is a product of a higher thermal and strain energy environment than in CZ rocks.

According to Sánchez-Navas and Galindo-Zaldivar (1993) the phyllosilicate structure favours the formation of kink-folds at the lattice scale since they act as multilayers that fold by flexural slip-mechanism as shown in Fig. 9. Due to this type of deformation, cracks open at the base of the kinks where slip is concentrated. These cracks are genetically very important because they increase intracrystalline permeability during deformation and produce pathways for solutions,

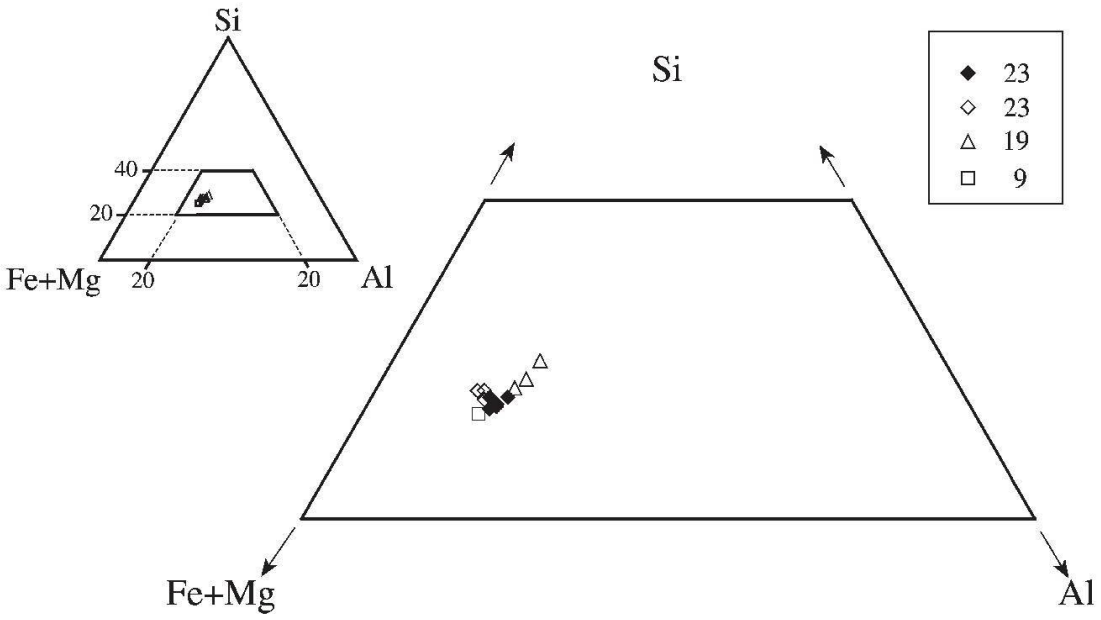


*Fig. 11* Compositional diagram of chlorites by EMPA (♦) and SEM. The analysed samples have been 23, 19 (WALZ) and 9 (CZ).

allowing the mass transfer required for metamorphic transformations, even within single crystals (Amouric, 1987; Sánchez-Navas and Galindo-Zaldivar, 1993; Zhao et al., 1999). Dissolution with subsequent neocrystallization will preferentially affect deformed grains, as phyllosilicate crystals of the WALZ samples, because they have a high internal strain energy (Wintsch, 1985). According to Giorgetti et al. (2000), the driving force of the textural changes seems to be due, in large part, to the deformation associated with the imperfections.

TEM images of muscovite usually show minimal strain contrast features in comparison with those of chlorite (e.g. Fig. 7 vs. Fig. 9). Different authors (Merriman et al., 1995; Arkai et al., 1996; Giorgetti et al., 2000) have observed the common presence of dislocations in chlorites and their absence in coexisting white mica. The contrasting response of different phyllosilicates to deformation was also observed to occur in biotite and associated muscovite (Bell and Wilson, 1981), where defect density in biotite increased with strain while muscovite did not show similar effects. The different responses to strain of dioctahedral and trioctahedral phyllosilicates has been correlated with the different activation energies of dislocations associated to the octahedral sheet (Merriman et al., 1995). In white micas, sub-grain development is quickly recovered by recrystallization, whereas chlorites retain strain-induced defects due to the slow rate of migration of dislocations that contribute to polygonization and segmentation of the crystals generating subgrains.

### *5.2. Phyllosilicate polytypes*

The only polytype detected in mica electron diffraction patterns of the Narcea Antiform has been the 2M polytype, regardless of the illitic or muscovitic character. The combination of low interlayer-cation contents and 2M polytypism is unusual in the white micas of low-grade metamorphic conditions. In prograde metamorphic environments, under anchizonal conditions the illite is characterized by a small size, composition with about 0.75–0.8 interlayer cations and $1M_d$ polytypism (Merriman and Peacor, 1999). In the case of CZ samples, white micas with typical illite compositions and typical muscovite polytypism have been analyzed but 1M and $1M_d$ polytypes have not been observed.

In the Narcea samples, different complex stacking sequences have been found in chlorite. Energetic differences between the different phyllosilicate polytypes are very small and the coexistence of several polytypes at the sample level has been described in diagenetic to epizone-grade rocks (López-Munguira and Nieto, 2000).

### *5.3. Chemical changes in slate-forming white micas: from external to internal zones*

The ubiquitous mineral assemblage, in both the CZ and WALZ, is quartz + white mica + chlorite ± albite. The bulk-rock compositions are also very similar (Table 1). Nevertheless, the change on chemical composition of micas is very significant because they are notably different in the two zones. The micas from foreland samples (CZ) are

highly heterogeneous including both illitic and muscovitic in composition; in contrast, the micas from hinterland samples (WALZ) have evolved to more homogeneous chemical compositions approaching the end-member muscovite (Fig. 10), although, they have not yet reached the characteristic homogeneity of higher metamorphic grade mineral phases.

The term illite is used in the IMA nomenclature for micas (Rieder et al., 1998) to designate interlayer-cation-deficient micas (< 0.85 a.f.u.). Illitic substitution has traditionally been related to low-temperature environment and cannot be ignored (Agard et al., 2001). However, it is difficult to define the compositional relationships between muscovite and illite in low-temperature rocks because of (1) the difficulty of obtaining uncontaminated analyses in small crystals, (2) the coincident effects of illitic component and possible contamination by smectite, and (3) cation loss during the measurement procedure. Therefore, very few data illustrate the relationship between the compositional changes in micas in the diagenesis and incipient metamorphism, most data being related to the smectite-to-illite transformation mechanism. Cuadros and Altaner (1998) determined an interlayer charge of 0.75 a.f.u. for the illite end-member in a study of illite/smectite from bentonites. The interlayer sum is in agreement with results found in other illite/smectite studies (Hower, 1981; Środoń et al., 1986; Lindgreen et al., 1991). An interdisciplinary research involving a variety of isotopic and mineralogical techniques was carried out by Hunziker et al. (1986) to document the progressive modification of illite into muscovite in a prograde metamorphic terrane. They concluded that there is a continuous structural and chemical reorganization rather than a recrystallization process during the transformation of illite to muscovite.

Livi et al. (1997) showed representative results of EMPA and AEM analyses of dispersed particles of dioctahedral phyllosilicates in low-grade metamorphosed shales. Although EMPA analyses might have been affected by contamination because of overlap with minerals other than mica, especially in the diagenetic-zone samples, and the AEM analyses were much less precise, as in our case, the two techniques nonetheless gave similar results (see Table 2). Livi et al. (1997) described a decrease in heterogeneity in mica analyses, an increasing interlayer charge and decreasing celadonite component as grade increased, that is, the same trends described above in the Narcea samples. This suggests that chemical compositional homogenization is the limiting process in forming equilibrated mica crystals.

The increase in metamorphic grade, higher strain values and time (Gutiérrez-Alonso, 1992, 1996; Gutiérrez-Alonso and Nieto, 1996) are very important factors not only in the development of textural features, but also in chemical evolution of white micas. The increasing K content in the interlayers and a richer aluminium composition point to an evolution towards micas near the end-member muscovite in the pelites of the internal domain (WALZ). These data confirm that these samples are near chemical equilibrium, which is absent in anchizonal samples, as proposed by Gutiérrez-Alonso and Nieto (1996) on the basis of a random pattern for the **b** parameter in the CZ. In contrast, only a small variation of this parameter was observed in the WALZ. Indirect estimation of the phengitic component from the **b** parameter is in agreement with measured values calculated from the chemical analyses. In addition, chemical analyses have shown that the compositional scattering among different samples from the foreland, as indicated by the **b** parameter, is also present among different grains at the sample level.

The high degree of chemical data heterogeneity for the CZ samples indicates an important effect of local composition at the beginning of the chemical transformations. Metamorphic evolution favours evolution towards homogeneity and a more muscovitic character of the micas and obliterates the effect of the detrital micas and smectites from the source area (Wybrecht et al., 1985). According to Merriman et al. (1990), the point at which neomorphic white mica becomes sufficiently abundant and well orientated to constitute a pervasive fabric depends partially on the initial lithology. The analyses of Narcea micas show that illitic compositions are present in the external domain and absent in the internal domain samples. The latter present only muscovitic compositions but in the former a continuous range of both kinds of mica compositions exist as a consequence of the absence of chemical equilibrium at the sample level. Therefore, whether illite has its own equilibrium field at lower temperatures than muscovites, or whether its presence is only a consequence of the low activation energy of these systems, is a question that remains unsolved in natural environments. In recent years, several attempts have been made to understand the formation and stability of end-member illite with respect to muscovite, over the temperature range of 100 to 250 °C through solid equilibration experiments (Yates and Rosenberg, 1997, 1998). These authors defined the composition of end-member illite 0.88 fixed K per $O_{10}(OH)_2$ and provided direct evidence for the stability of end-member il-

lite with respect to illite/smectite and muscovite in the temperature range of the study.

### 5.4. Composition and mixed-layering of chlorite

In contrast with the textural evolution, chlorite compositions are more homogeneous than those of micas. Nevertheless, their more strained, defective character and the contamination by vermiculite (Fig. 5) and/or dioctahedral micas in CZ samples have prevented a clear interpretation of their chemical evolution with grade. The presence of minor interstratified vermiculite layers in the chlorite packets of sample 2 (CZ) could be attributed to corrensite domains not completely transformed to chlorite. Nonetheless, a re-evaluation of the XRD diagrams of the samples studied by Gutiérrez-Alonso and Nieto (1996) has not shown a clear relationship between the presence of this interstratification and the metamorphic grade (unpublished data). The apparently random presence of minor quantities of expandable layers is therefore more probably related with surface weathering or retrograde diagenetic effects similar to those described by Zhao et al. (1999) in clay minerals in the Precambrian Freda sandstone (Wisconsin) and Nieto et al. (1994) in chlorites of Betic red shales (Spain). These authors postulated an introduction of a pore fluid that produced a reactive environment in which chlorite would become specially sensitive.

7-Å layers are present in the anchizone samples. Amouric et al. (1988) and Guthrie and Veblen (1990) concluded that their presence may be associated with dynamic diffraction effects or real layers of berthierine. These occurrences have frequently been described in diagenetic and very low-grade samples (e.g. Jiang et al., 1992) and are the consequence of the absence of mineral equilibrium formed under low-temperature conditions. Abad-Ortega and Nieto (1995) showed that berthierine is a metastable polymorph of chlorite and that both polymorphs can coexist when the sample has not reached equilibrium.

### 5.5. Concluding remarks

From the comparative study of the microtextural and microanalytical features of these rocks, a parallel texture-compositional evolution from the external domain (CZ) to the internal domain (WALZ) can be deduced in the collisional setting of the Variscan orogen.

As indicated by the IC values, a change in metamorphic grade, from anchizone to epizone, exists between the two foreland samples (Fig. 1), but this evolution is not parallel to the chemical composition trend (Fig. 10). That is, the transition between rocks that still conserve some sedimentary features and illitic-muscovitic compositions towards typical metamorphic rocks near chemical equilibrium and muscovitic compositions happens within the epizone and close to the foreland-hinterland boundary of the Variscan orogen in the NW Iberian Massif. Samples such as number 9 present an IC corresponding to epizone, but without the textural and chemical features of common metamorphic rocks. Therefore the effects of tectonic stress are fundamental both in the development of a metamorphic texture and the approach to chemical equilibrium.

The slow rates of low-grade metamorphic processes are responsible for the absence of chemical equilibrium in the foreland rocks, as indicated by their textural features and heterogeneous compositions, which nonetheless imply at least the initial effects of an increase in pressure and temperature. In spite of their 2M polytype, micas from the external zone still present a significant degree of illitic substitution. In comparison, the internal zone underwent higher temperatures and consequently the crystallization processes and incipient homogenization are more evident.

**Acknowledgements**

We thank M.M. Abad-Ortega and A. González from the Centro de Instrumentación Científica (C.I.C.) of the Universidad de Granada for their assistance in using the HRTEM and SEM, respectively. We are grateful to Christine Laurin for revising the English text. Thanks to N. Velilla for useful discussion and ideas. The critical reviews and very helpful comments and suggestions of D.R. Peacor, S. Schmidt, L. Warr and an anonymous reviewer have notably improved the quality of the paper. This research was supported by Research Projects n$^{os}$ BT2000-0582 and BTE2000-1490-C02-01 and FPI research grant to I.A., all from the Spanish Ministry of Science and Technology and Research Group RNM-0179 of the Junta de Andalucía.

**References**

Abad, I., Nieto, F. and Velilla, N. (2002): Chemical and textural characterisation of diagenetic-low-grade metamorphic phyllosilicates in turbidite sandstones of the South Portuguese Zone: A comparison between metapelites and sandstones. *Schweiz. Mineral. Petrogr. Mitt.* **82**, 303–324.

Abad-Ortega, M.M. and Nieto, F. (1995): Genetic and chemical relationship between berthierine, chlorite and cordierite in nodules associated to granitic pegmatites of Sierra Albarrana (Iberian Massif, Spain). *Contrib. Mineral. Petrol.* **120**, 327–336.

Agard, P., Vidal, O. and Goffé, B. (2001): Interlayer and Si content of phengite in HP-LT carpholite-bearing metapelites. *J. Metamorphic Geol.* **19**, 477–493.

Amouric, M. (1987): Growth and deformation defects in phyllosilicates as seen by HRTEM. *Acta Cryst.* **B43**, 57–63.

Amouric, M., Gianetto, I. and Proust, D. (1988): 7, 10 and 14 Å mixed-layer phyllosilicates studied structurally by TEM in pelitic rocks of the Piemontese zone (Venezuela). *Bull. Minéral.* **111**, 29–37.

Árkai, P., Merriman, R.J., Roberts, B., Peacor, D.R. and Toth, M. (1996): Crystallinity, crystallite size and lattice strain of illite-muscovite and chlorite: comparison of XRD and TEM data for diagentic to epizonal pelites. *Eur. J. Mineral.* **8**, 1119–1137.

Banfield, J.F. and Murakami, T. (1998): Atomic-resolution transmission electron microscope evidence for the mechanism by which chlorite weathers to 1:1 semi-regular chlorite-vermiculite. *Am. Mineral.* **83**, 348–357.

Bell, I.A. and Wilson, C.J.L. (1981): Deformation of biotite and muscovite: TEM microstructure and deformation model. *Tectonophysics* **78**, 201–228.

Cuadros, J. and Altaner, S.P. (1998): Characterization of mixed-layer illite-smectite from bentonites using microscopic, chemical, and X-ray methods: Constraints on the smectite-to-illite transfomation mechanism. *Am. Mineral.* **83**, 762–774.

Dallmeyer, R.D., Martínez Catalán, J.R., Arenas, R., Gil Ibarguchi, I., Gutiérrez-Alonso, G., Farias, P., Bastida, F. and Aller, J. (1997): Diachronous Variscan tectonothermal activity in the NW Iberian Massif: Evidence from $^{40}Ar/^{39}Ar$ dating of regional fabrics. *Tectonophysics* **277**, 307–337.

Fernández-Suárez, J., Gutiérrez-Alonso, G., Jenner, G.A. and Tubrett, M.N. (2000): New ideas on the Proterozoic-Early Palaeozoic evolution of NW Iberia: insights from U-Pb detrital zircon ages. *Precambrian Research* **102**, 185–206.

Giorgetti, G., Memmi, I. and Peacor, D.R. (2000): Retarded illite crystallinity caused by stress-induced subgrain boundaries in illite. *Clay Minerals* **35**, 693–708.

Guthrie, G.D.Jr. and Veblen, D.R. (1990): Interpreting one-dimensional high-resolution transmission electron micrographs of sheet silicates by computer simulation. *Am. Mineral.* **75**, 276–288.

Guidotti, C.V. and Sassi, F.P. (1986): Classification and correlation of metamorphic facies series by means of muscovite b data from low-grade metapelites. *Neues Jahrb. Mineral. Abh.* **153**, 363–380.

Guidotti, C.V., Yates, M.G., Dyar, M.D. and Taylor M.E. (1994): Petrogenetic implications of the $Fe^{3+}$ content of muscovite in pelitic schists. *Am. Mineral.* **79**, 793–795.

Guidotti, C.V. and Sassi, F.P. (1998): Petrogenetic significance of Na-K white mica mineralogy: Recent advances for metamorphic rocks. *Eur. J. Mineral.* **10**, 815–854.

Gutiérrez-Alonso, G. (1992): El Antiforme del Narcea y su relación con los mantos occidentales de la Zona Cantábrica. Unpublished PhD Thesis. University of Oviedo.

Gutiérrez-Alonso, G. (1996): Strain partitioning in the footwall of the Somiedo Nappe: structural evolution of the Narcea Tectonic Window, NW Spain. *J. Struct. Geol.* **18**, 1217–1230.

Gutiérrez-Alonso, G. and Nieto, F. (1996): White-mica "cristallinity", finite strain and cleavage development across a large Variscan structure, NW Spain. *J. Geol. Soc. London* **153**, 287–299.

Ho, N., Peacor, D.R. and Van der Pluijm, B.A. (1995): Reorientation mechanisms of phyllosilicates in the mudstone-to-slate transition at Lehigh Gap, Pennsylvania. *J. Struct. Geol.* **17**, 345–356.

Ho, N., Peacor, D.R. and Van der Pluijm, B.A. (1996): Contrasting roles of detrital and authigenic phyllosilicates during slaty cleavage development. *J. Struct. Geol.* **18**, 615–623.

Hower, J. and Mowatt, T.C. (1966): The mineralogy of illites and mixed-layer illites-montmorillonites. *Am. Mineral.* **51**, 825–854.

Hower, J. (1981): Shale diagenesis. In: Longstaffe, F.J. (ed.): Clays and the Resource Geologist, Short Course Handbook **7**, *Mineral. Assoc. Canada,* 60–80.

Hunziker, J.C., Frey, M., Clauer, N., Friedrichsen, H., Flehmig, W., Hochstrasser, K., Roggwiler, P. and Schwander H. (1986): The evolution of illite to muscovite: mineralogical and isotopic data from the Glarus Alps, Switzerland. *Contrib. Mineral. Petrol.* **92**, 157–180.

Inoue, A. and Utada, M. (1983): Further investigations of a conversion series of dioctahedral mica/smectites in the Shinzan hydrothermal alteration area, northeast Japan. *Clays Clay Mineral.* **31**, 401–412.

Jiang, W., Peacor, D.R. and Slack, J.F. (1992): Microstructures, mixed layering, and polymorphism of chlorite and berthierine in the Kidd Creek massive sulfide deposit, Ontario. *Clays Clay Mineral.* **40**, 501–514.

Julivert, M. (1971): L'evolution structurale de l'arc asturien. In: Histoire Structurale du Golfe de Gascone 2, Inst. Fr. Pétrole Paris, 1-28.

Kerrich, R. (1977): An historical review and synthesis of research on pressure solution. *Zentralb. Geol. Palaeont.* **I**, 512–550.

Knipe, J.R. and White, S.H. (1977): Microstructural variation of an axial plane cleavage around a fold – a H.V.E.M. study. *Tectonophysics* **39**, 355–380.

Knipe, J.R. (1981): The interaction of deformation and metamorphism in slates. *Tectonophysics* **78**, 249–272.

Kübler, B. (1968): Evaluation quantitative du métamorphisme par la cristallinité de l'illite. *Bull. C. Rech. Pau-SNPA* **2**, 385–397.

Lee, J.H., Peacor, D.R., Lewis, D.D. and Wintsch, R.P. (1986): Evidence for syntectonic crystallization for the mudstone to slate transition at Lehigh Gap, Pennsylvania, U.S.A. *J. Struct. Geol.* **8**, 767–780.

Lindgreen, H., Jacobsen, H. and Jakobsen, H. (1991): Diagenetic structural transformations in North Sea Jurassic illite-smectite. *Clays Clay Mineral.* **39**, 54–69.

Livi, K.J.T., Veblen, D.R., Ferry, J.M. and Frey, M. (1997): Evolution of 2:1 layered silicates in low-grade metamorphosed Liassic shales of Central Switzerland. *J. Metamorphic Geol.* **15**, 323–344.

López-Munguira, A. and Nieto, F. (2000): Transmission electron microscopy study of very low-grade metamorphic rocks in Cambrian sandstones and shales, Ossa-Morena Zone, Southwest Spain. *Clays Clay Mineral.* **48**, 213–223.

Merriman, R.J., Roberts, B. and Peacor, D.R. (1990): A transmission electron microscope study of white mica crystallite size distribution in a mudstone to slate transitional sequence, North Wales, UK. *Contrib. Mineral. Petrol.* **106**, 27–40.

Merriman, R.J., Roberts, B., Peacor, D.R. and Hirons, R. (1995): Strain related differences in the crystal growth of white mica and chlorite: a TEM and XRD study of the development of metapelitic microfabrics in the Southern Uplands thrust terrane, Scotland. *J. Metamorphic Geol.* **13**, 559–576.

Merriman, R.J. and Peacor, D.R. (1999): Very low-grade metapelites: mineralogy, microfabrics and measuring reaction progress. In: Frey, M. and Robinson, D. (eds.): Low grade-metamorphism, Blackwell Science Oxford, 10–60.

Nieto, F., Velilla, N., Peacor, D.R. and Ortega, M. (1994): Regional retrograde alteration of sub-greenschist facies chlorite to smectite. *Contrib. Mineral. Petrol.* **115**, 243–252.

Nieto, F. (1997): Chemical composition of metapelitic chlorites: X-ray diffraction and optical property approach. *Eur. J. Mineral.* **9**, 829–841.

Pouchou, J.L. and Pichoir, F. (1985): "PAP" (f) (r) (t) procedure for improved quantitative microanalysis. In: Armstrong, J.T. (ed.): Microbeam Analysis, San Francisco Press, San Francisco, 104 pp.

Rieder, M., Cavazzini, G., D'Yakonov, Y.S., Kamanetskii, V.A.F., Gottardi, G., Guggenheim, S., Koval, P.K., Müller, G., Neiva, A.M.R., Radoslovich, E.W., Robert, J.L., Sassi, F.P., Takeda, H., Weiss, Z. and Wones, D.R. (1998): Nomenclature of the micas. *Can. Mineral.* **36**, 905–912.

Sánchez-Navas, A. and Galindo-Zaldivar, J. (1993): Alteration and deformation microstructures of biotite from plagioclase-rich dykes (Ronda Massif, S. Spain). *Eur. J. Mineral.* **5**, 245–256.

Sorby, H.C. (1853): On the origin of slaty cleavage. *Edinburgh New Phil. J.* **55**, 137–148.

Środoń, J., Morgan, D.J., Eslinger, E.V., Eberl, D.D. and Karlinger, M.R. (1986): Chemistry of illite/smectite and end-member illite. *Clays Clay Mineral.* **34**, 368–378.

Sutton, S.J. (1989): Orientation-dependent "metamorphic grade" in phyllosilicates belonging to a slaty cleavage fabric. *J. Geol.* **97**, 197–208.

Taylor, S.R. and McLennan, S.M. (1985): The continental crust: its composition and evolution. Blackwell, Oxford, 312 pp.

Van der Pluijm, B.A., Ho, N.C. and Peacor, D.R. (1998): Contradictions of slate formation resolved? *Nature* **392**, 348.

Weaver, C.E. (1965): Potassium content of illite. *Science* **147**, 603–605.

Weber, K. (1981): Kinematic and metamorphic aspects of cleavage formation in very low-grade metamorphic slates. *Tectonophysics* **78**, 291–306.

White, S.H. and Knipe, R.J. (1978): Microstructure and cleavage development in selected slates. *Contrib. Mineral. Petrol.* **66**, 165–174.

Wintsch, R.P. (1985): The possible effects of deformation on chemical processes in metamorphic fault zones. In: Thompson, A.H. and Rubie, D.C. (eds.): Metamorphic reactions: kinetics, textures, and deformation, Springer New York. 251–268.

Wintsch, R.P., Kvale, C.M. and Kisch, H.J. (1991): Open-system, constant-volume development of slaty cleavage, and strain-induced replacement reactions in the Martinsburg Formation, Lehigh Gap, Pennsylvania. *Bull. Geol. Soc. Am.* **103**, 916–927.

Wood, D.S. (1974): Current views of the development of slaty cleavage. *Annu. Rev. Earth Planet. Sci.* **2**, 369–401.

Wybrecht, E., Duplay, J., Piqué, A. and Weber, F. (1985): Mineralogical and chemical evolution of white micas and chlorites, from diagenesis to low-grade metamorphism; data from various size fractions of greywackes (Middle Cambrian, Morocco). *Mineral. Mag.* **49**, 401–411.

Yates, D.M. and Rosenberg, P.E. (1997): Formation and stability of endmember illite: II. Solid equilibration experiments at 100 to 250 °C and Pv,soln. *Geochim. Cosmochim. Acta* **61**, 3135–3144.

Yates, D.M. and Rosenberg, P.E. (1998): Characterization of neoformed illite from hydrothermal experiments at 250 °C and Pv,soln: An HRTEM/ATEM study. *Am. Mineral.* **83**, 1199–1208.

Zhao, G., Peacor, D.R. and McDowell, S.D. (1999): "Retrograde diagenesis" of clay minerals in the Precambrian Freda sandstone, Wisconsin. *Clays Clay Mineral.* **47**, 119–130.

Received 5 May 2002
Accepted in revised form 24 November 2002
Editorial handling: S. Th. Schmidt and M. Engi